The 15th International Symposium on Magnetic Bearings, August 3-6, 2016, Mojiko Hotel, Kitakyushu, Japan

ISMB15

Unbalance force observer and compensator of magnetic bearings supporting centrifugal compressor

Kexiang LI*, Zhiquan DENG*[a], Chengzi LIU*, Jie ZHOU*, Jiaxi HE* and Jiaqiang NING**

* College of Automation Engineering, Nanjing University of Aeronautics and Astronautics
Jiangning District, Nanjing, 211100, P.R.China
[a] E-mail: dzq@nuaa.edu.cn
** Nanjing Engineering Institute of Aircraft Systems, AVIC
Jiangning District, Nanjing, 211100, P.R.China

Abstract

Magnetically suspended centrifugal compressors own unbalance forces in all degrees of freedom. The forces in radial directions are mainly derived from residual unbalance mass, and in axial directions are from shocking loads. These disturbances all can be observed using extended state observer, with which the unbalance forces can be compensated rapidly. In order to increase the precision of estimation and compensation, relevant parameters of magnetic bearings were theoretically and experimentally determined. The characteristics of the observer were studied through theoretical analysis and simulations. Additionally, a method, which can verify estimation accuracy was adopted in our research. At last, the unbalance force observation and compensation were realized on a suspended centrifugal compressor, which can be concluded that ESO owns fine disturbance rejection ability for active magnetic bearings.

Keywords : Active Magnetic Bearing, Extended State Observer, Unbalance Force Compensation, Parameter Determination, Stability Verification

1. Introduction

Active magnetic bearings (AMBs) can support rotor shafts using controlled electromagnetic forces without any mechanical contacts, which bring out some benefits such as low-loss, long-life, low-noise, and even non-lubrication. These advantages of AMBs have led to applications mainly in vacuum systems, cleanroom systems, machine tools, turbo-machinery and so on. Actually, the main application area of AMBs is turbo-machinery covering from small turbo-molecular pumps up to turbo-generators and compressors in the megawatt range (Schweitzer and Maslen, 2009).

For the sake of high rotational speed with high power density, AMB is a good choice of bearing for centrifugal compressors. The whole rotor shaft with turbine disks can be suspended by AMBs, and be directly driven by electrical machines. However, disturbances are common for a compressor rotor shaft, not only in radial but also in axial directions. In radial directions, centrifugal forces owing to unbalance masses cannot be neglected, especially when rotor shafts spin in high speed. Besides, turbine disks draw fluid in axial directions, so load forces in this directions will vary when rotational speed changes. Last but not least, if load or rotational speed requires to be changed rapidly, shafts will suffer from abrupt disturbances in all directions. Consequently, a method which can reject abrupt disturbances is significant.

The PID algorithm is commonly used in levitation feedback control because of its ease of tuning and good steady state performance. Nevertheless, PID algorithm owns some inherent demerits that there exists contradictions between rapidity and overshoot; the integrator in PID can only reject constant disturbances but not dynamic ones (Han, 2002). To make up this deficiency, Active Disturbance Rejection Control (ADRC) technology was proposed (Han, 1998). The core technology of ADRC is Extended State Observer (ESO), which is adopted to estimate all the disturbances on the plant. And then, the estimation value is compensated into the controller to realize disturbance rejection.

ESO has been realized in controllers for suspension systems by many researchers. (Alexander, et al., 2008) used ESO to control rotor shaft position of NASA's High Speed Shaft Flywheel to enhance the robustness of the controller. ESO was also be adopted in self-bearing motors to compensate disturbances and simplify the levitation decoupling algorithm (Wang and Ding, 2011) (Wang and He, 2012). Some scholars also realized ESO in suspension position controller for precise planar magnetic bearings (Zhou, et al., 2010) (Zhou, et al., 2008).

The literature owns many theoretical analyses and simulation results, but few experimental verifications. Some fundamental research and tests have also been done on a suspended machine (Li, et al., 2015a, 2015b). However, it lacked estimation accuracy verifications of ESO on real platforms, the same as above literature with experiment. As a result, a method is used to verify the estimation accuracy, based on which the load force estimation and disturbance rejection of suspended compressors can be carried out more easily and correctly.

This paper is organized as follows. ESO suitable for AMB is designed and its parameter tuning method and stability analysis are elaborated in Section 2. In Section 3, related parameters are determined on a suspended compressor test rig to help enhance estimation accuracy. In Section 4, the performance and characteristics of ESO are studied through simulation. At last, experimental verification results are shown in Section 5.

2. Design of disturbance observer and compensator

For each levitation degree of freedom, ESO can take all interferences as disturbances, including external disturbance forces from abrupt load variation or outside perturbations, and even coupling forces from other degrees of freedom. Then all of the disturbances can be compensated simultaneously. Therefore, ESO and compensators of AMB can be established based on decentralized levitation feedback control, as shown in Fig.1.

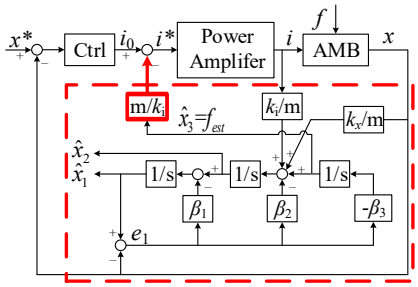

Fig.1 Control block diagram of ESO for AMB. ESO (in red dashed box) and compensators (plotted with red heavy line) are added into a decentralized levitation feedback control for one degree of freedom. x^* and x denote given and actual displacements respectively; i^* and i denote given and actual currents respectively; f denotes actual disturbances on this degree of freedom; f_{est} denotes estimated disturbances from ESO. Steady levitation controller is denoted by Ctrl.

2.1 Modeling of AMB

Permanent-magnet-based axial and radial AMB is adopted in the suspended compressor, which can simultaneously levitate the rotor shaft in three degrees of freedom. According to mathematic model of suspension forces of AMB and its linearization at operating point, suspension force in each degree of freedom can be formulated as:

$$f(x,i) = k_s x + k_i i \tag{1}$$

where the constants k_s (N/m) and k_i (N/A) are commonly called force/displacement factor (position stiffness) and force/current factor (current stiffness). x and i are values of displacement fluctuation and control current.

Concerning disturbances shown in Fig.1, the right side of Eq.(1) can be added with a term f, which denotes external disturbances or coupling forces from other degrees of freedom. Then motion state equation of this degree of freedom can be derived with an extended state $x_3 = f/m_{eq}$ added as:

$$\begin{cases} \dot{x}_1 = x_2 \\ \dot{x}_2 = k_i i/m_{eq} + k_s x_1/m_{eq} + x_3 \\ \dot{x}_3 = h \\ y = x_1 \end{cases} \tag{2}$$

where x_1 and x_2 denote displacement and its differential; x_3 denotes accelerated speed derived from disturbances which is to be estimated. Note that m_{eq} is equivalent mass of this degree of freedom, not total mass of the rotor shaft.

Then corresponding state space model can be derived as:

$$\begin{cases} \dot{\boldsymbol{x}} = \boldsymbol{A}\boldsymbol{x} + \boldsymbol{B}u + \boldsymbol{D}y + \boldsymbol{E}h \\ y = \boldsymbol{C}\boldsymbol{x} \end{cases} \quad \left(\boldsymbol{A} = \begin{bmatrix} 0 & 1 & 0 \\ 0 & 0 & 1 \\ 0 & 0 & 0 \end{bmatrix} \boldsymbol{B} = \begin{bmatrix} 0 \\ k_i/m_{eq} \\ 0 \end{bmatrix} \boldsymbol{C} = \begin{bmatrix} 1 & 0 & 0 \end{bmatrix} \boldsymbol{D} = \begin{bmatrix} 0 \\ k_s/m_{eq} \\ 0 \end{bmatrix} \boldsymbol{E} = \begin{bmatrix} 0 \\ 0 \\ 1 \end{bmatrix} \right) \tag{3}$$

where $\boldsymbol{B}u$ and $\boldsymbol{D}y$ are the known values, since u and y can be easily obtained by transducers, and the constants m_{eq}, k_i and k_s can be determined as elaborated in Section 3.

2.2 Extended state observer

Based on motion state equation of AMB as Eq.(3), ESO can be designed as follows:

$$\begin{cases} \dot{\hat{\boldsymbol{x}}} = \boldsymbol{A}\hat{\boldsymbol{x}} + \boldsymbol{B}u + \boldsymbol{D}y + \boldsymbol{F}\left(y - \hat{y}\right) \\ \hat{y} = \boldsymbol{C}\hat{\boldsymbol{x}} \end{cases} \qquad \left(\boldsymbol{F} = \begin{bmatrix} \beta_1 & \beta_2 & \beta_3 \end{bmatrix}^T\right) \tag{4}$$

where $\hat{\boldsymbol{x}}$ is estimation values of $\boldsymbol{x}$; the coefficient matrix $\boldsymbol{F}$ needs to be tuned for high observation accuracy. From Eq.(4), we can conclude that the inputs of ESO are u=i and y=x_1.

Subtracting Eq.(3) from Eq.(4), error of state estimation can be derived as:

$$\dot{\boldsymbol{e}} = \left(\boldsymbol{A} - \boldsymbol{F}\boldsymbol{C}\right)\boldsymbol{e} - \boldsymbol{E}\,h \tag{5}$$

When ESO is stable, Eq.(5) will converge to 0. Then we can get error equation $\boldsymbol{e} = \mathrm{diag}\begin{bmatrix} -\beta_3^{-1} & -\beta_1\beta_3^{-1} & -\beta_2\beta_3^{-1} \end{bmatrix} h$, from which we can conclude that if β_3 is much bigger, $\boldsymbol{e}$ will converge to 0. Then it will be derived that $\hat{\boldsymbol{x}} \approx \boldsymbol{x}$. Consequently, $\hat{x}_3$ converges to the accelerated speed derived from disturbances, which is the value we want to estimate. Then, disturbances can be compensated rapidly through subtracting estimated values in control current as:

$$i^* = i_0 - \hat{x}_3\, m_{eq} / k_i \tag{6}$$

Above all, based on the model of ESO, control block diagram of it is constructed as dashed box in Fig.1. Through extracting actual control current and displacement by transducers, ESO will estimate disturbances to reject.

2.3 Parameter tuning method

The parameter matrix of ESO has three unknown parameters, so the tuning method should be studied to simplify the process. Bandwidth concept was introduced in (Gao, 2006) to realize the simplification, according to which characteristic polynomial of the error equation is $\left(s^3 + \beta_1 s^2 + \beta_2 s + \beta_3\right)$. And based on Lyapunov's stability criterion, that control system will be stable when all the eigenvalues' real parts of characteristic polynomial are negative. Besides, transient process will be ideal when 3rd order characteristic polynomial is as follows:

$$\left(\boldsymbol{s} + \omega\right)^3 = \boldsymbol{s}^3 + 3\omega\boldsymbol{s}^2 + 3\omega^2\boldsymbol{s} + \omega^3 = \boldsymbol{s}^3 + \beta_1\boldsymbol{s}^2 + \beta_2\boldsymbol{s} + \beta_3 \tag{7}$$

Therefore, we can let β_1=3ω, β_2=$3\omega^2$ and β_3=ω^3, which will make ESO own only one unknown parameter.

2.4 Stability analysis

In order to realize digital control, the model of ESO must be discretized for stability verification. Based on Eq.(5), the discrete form of the error function can be written as follows:

$$\begin{cases} \boldsymbol{e}(k+1) = \left(\boldsymbol{M} - \boldsymbol{L}\boldsymbol{C}\right)\boldsymbol{e}(k) \\ \tilde{y}(k) = \boldsymbol{C}\boldsymbol{e}(k) \end{cases} \qquad \left(\boldsymbol{M} = \begin{bmatrix} 1 & T & 0 \\ 0 & 1 & T \\ 0 & 0 & 1 \end{bmatrix},\ \boldsymbol{L} = T\boldsymbol{F}\right) \tag{8}$$

where T is the control period of controller. On the basis of the observability criteria that, if the control period is not zero, the equation below is true, which means the system is observable.

$$rank\begin{bmatrix} \boldsymbol{C} \\ \boldsymbol{C}\boldsymbol{M} \\ \boldsymbol{C}\boldsymbol{M}^2 \end{bmatrix} = rank\begin{bmatrix} 1 & 0 & 0 \\ 1 & T & 0 \\ 1 & 2T & T^2 \end{bmatrix} = 3 \tag{9}$$

The characteristic polynomial of $\left(\boldsymbol{M} - \boldsymbol{L}\boldsymbol{C}\right)$ is expressed as follows:

$$z^3 + \left(T\beta_1 - 3\right)z^2 + \left(-T^2 d + T^2\beta_2 - 2T\beta_1 + 3\right)z + \left(dT^2 + T^3\beta_3 - T^2\beta_2 + T\beta_1 - 1\right) \tag{10}$$

According to the theory, i.e., if the roots of the characteristic matrix are all in the unit disc, the observer will be stable. Combined with $\beta_1=3\omega$, $\beta_2=3\omega^2$ and $\beta_3=\omega^3$, the stability domain can be derived as $0<\omega<2/T$.

Above all, with the parameter configuration and the stability range, the parameter tuning process is more normative.

3. Parameter determination

3.1 Suspended compressor setup

Performance verification was carried out on an AMB supporting centrifugal compressor as shown in Fig.2. The pair of permanent-magnet-based axial and radial AMBs can suspend the rotor shaft in five degrees of freedom, and the rotation motion about the z-axis is driven by a 11.5kW brushless DC motor. It is essential that the rated rotational speed of the electric machine is 1kHz (60,000r/min) which is much lower than the first bending frequency of the rotor shaft (1.58kHz), so the rotor can be regarded as a rigid rotor in its operation range.

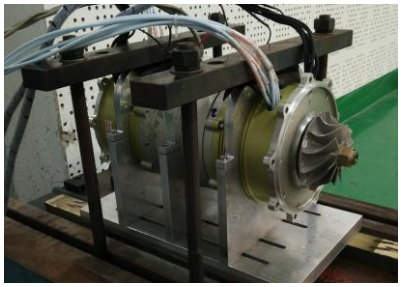

Fig.2 AMB supporting centrifugal compressor. Two identical AMBs are equipped symmetrically, and an electrical motor is in the middle to drive. Turbine disks can be assembled at each end of the shaft.

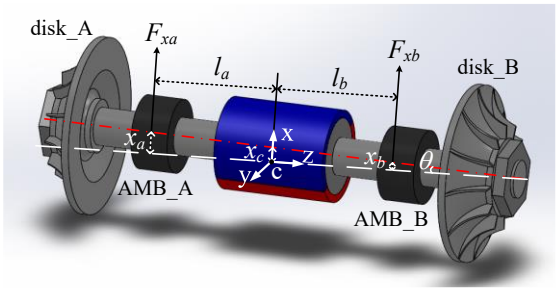

Fig.3 Schematic diagram of suspended compressor rotor shaft (moving in x-direction). The dashed (white) line denotes clearance centerline of AMB, and the dot-dash (red) line denotes journal centerline of AMB.

3.2 Equivalent mass

First of all, the moment of inertia about each direction is obtained through 3-Dimension finite element analysis, as shown in Tab.1. The gyroscopic effects of the suspended rotor shaft can be neglected, since the shaft is spindly ($I_{z0}<<I_{x0}=I_{y0}$). That is to say, the motions in x-direction and y-direction have little interaction with each other, and the calculation of equivalent mass can be carried out in each direction separately.

Table 1 Some related parameters of the suspended rotor shaft

Parameter	Value
l_a/m	$8.395*10^{-2}$
l_b/m	$8.405*10^{-2}$
m/kg	3.54
I_{x0}/kg×m^2	2.2487×10^{-2}
I_{y0}/kg×m^2	2.2487×10^{-2}
I_{z0}/kg×m^2	1.0869×10^{-3}

Table 2 Some related parameters of the AMB

Parameter		Radial value	Axial value
Current stiffness	k_i/N×A^{-1}	67	46.4
Position stiffness	k_s/N×m^{-1}	2.38×10^5	5×10^5
Equivalent mass	m_{eq}/kg	1.68	3.54
P-coefficient	K_P	0.5	1.17
I-coefficient	K_I	6	10.2
D-coefficient	K_D	0.0016	0.004
Parameter in ESO	ω	17000	17000

The equivalent mass of axial degree of freedom is obviously equal to mass of the total shaft. And in radial degree of freedom, calculation in x-direction is taken as an example, which is illustrated in Fig.3. Spans from mass centers of the rotor shaft to each AMB are l_a and l_b respectively; displacements in x-direction of AMB_A rotor, AMB_B rotor and mass center of total rotor shaft are denoted as x_a, x_b and x_c, respectively. Supposing suspension forces of the two AMBs in x-direction are F_{xa} and F_{xb} respectively; mass of the total rotor shaft is m; and angle of rotation about y-axis is θ .

Neglecting gyroscopic effects as mentioned before, dynamical equation of the rotor shaft in x-direction can be established below, and the geometrical relationships are accessible:

$$\begin{cases} m\ddot{x}_c = F_{xa}+F_{xb} \\ I_{y0}\ddot{\theta} = F_{xa}l_a - F_{xb}l_b \end{cases} \quad \left(\begin{cases} x_c = \left(x_a l_b + x_b l_a\right)/\left(l_a+l_b\right) \\ \theta = \left(x_a - x_b\right)/\left(l_a+l_b\right) \end{cases} \right) \tag{11}$$

With design parameters and 3-Dimension model of this suspended rotor shaft, related parameters are calculated out, as

shown in Tab.1. Subsequently, the accelerated speed of AMBs can be derived as:

$$\begin{cases} \ddot{x}_a = \left[\left(I_{y0} + l_a^2 m\right)F_{xa} + \left(I_{y0} - l_a l_b m\right)F_{xb}\right] / \left(mI_{y0}\right) = 0.596F_{xa} - 0.031F_{xb} \\ \ddot{x}_b = \left[\left(I_{y0} - l_a l_b m\right)F_{xa} + \left(I_{y0} + l_b^2 m\right)F_{xb}\right] / \left(mI_{y0}\right) = -0.031F_{xa} + 0.597F_{xb} \end{cases} \tag{12}$$

from which equivalent mass of each radial degree of freedom can be derived as m_a=m_b=1.68kg.

3.3 Current and position stiffness

In order to determine accurate stiffness values, we test them on a suspended centrifugal compressor rig. In the first place, we exert different constant disturbances on each degree of freedom with the rotor being at equilibrium position, i.e. x=0 in Eq.(1). A set of load forces and corresponding currents will be obtained, as illustrated in Fig.4. Then we can obtain the current stiffness of radial and axial degree of freedom, which are 67N/A and 46.4N/A respectively.

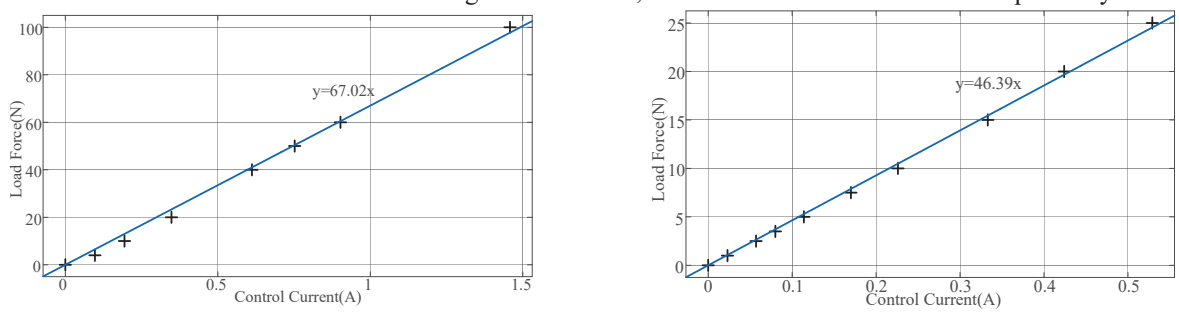

Fig.4 Current stiffness fitting curve of radial (left) and axial (right) degree of freedom. Owing to symmetry, a pair of identical forces at each end of the rotor shaft in radial directions is exerted on the rotor shaft. And load forces with different values are exerted in z-direction on the compressor, which is vertically placed. Then a set of load forces and corresponding control currents of each degree of freedom can be obtained.

The second step is to change given displacement at different position when external disturbances are absent, i.e. f=0 in Eq.(1). Then we can get the linear relationship between current stiffness and position stiffness, and then position stiffness can be derived easily. Based on Fig.5, the values of position stiffness in radial and axial degree of freedom are derived, which are 238N/mm and 500N/mm respectively.

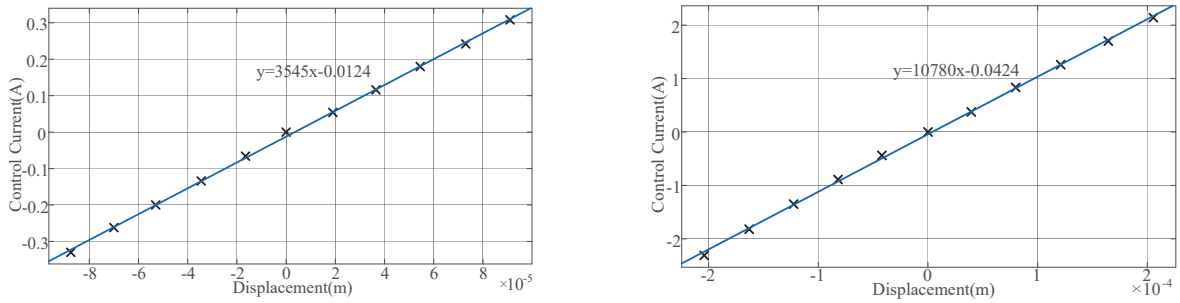

Fig.5 Relationship between current and position stiffness in radial (left) and axial (right) degree of freedom. Given displacement of radial and axial degree of freedom is changed respectively. And then a set of displacements and control currents can be obtained.

4. Simulation verification

With values of stiffness and equivalent mass, models of AMB and controller systems are established in Matlab/Simulink. Subsequently, coefficient of PID controller is tuned in order to realize levitation feedback stable, and then ESO is added into the system with a parameter ω to be adjusted. These parameters of controller are all shown in Tab.2. The estimated disturbances will be compensated into original feedback control until the estimation accuracy of ESO is verified. Below are results and analyses of simulation.

4.1 Results of simulation

The first step is to realize open-loop disturbance estimation through adjusting the parameter ω in ESO. In radial degree of freedom, sinusoidal disturbances with variable frequencies are exerting to AMB, which are simulated as rapid speed changes. The speed changes from 10,000 to 15,000 r/min at 0.04s, and the amplitude of disturbance force from 65.8N to 148N. In axial degree of freedom, step disturbances (±50N) are simulated as rapid load force changes. The

simulation results are shown in Fig.6, which can be seen that the estimation is accurate.

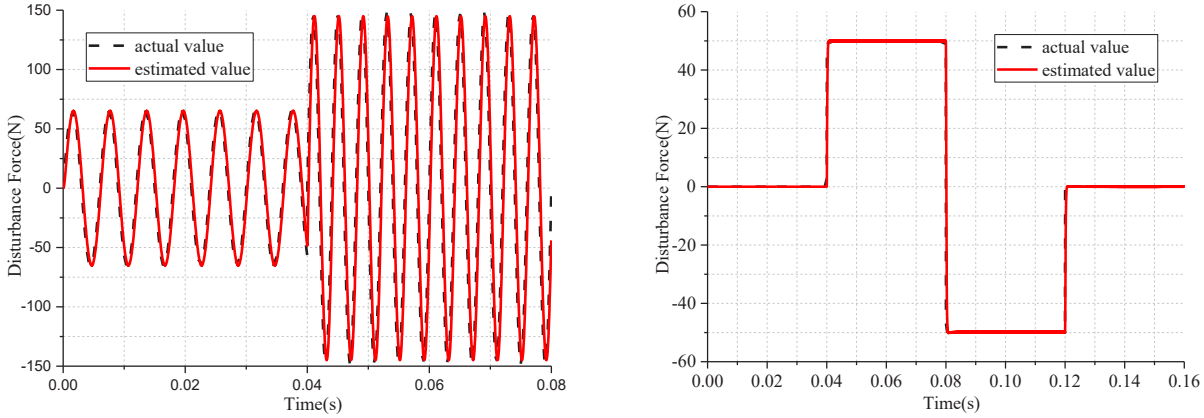

Fig.6 Simulation results of disturbance estimation in radial (left) and axial (right) degree of freedom. Actual and estimated values are plotted with the dashed (black) and solid (red) curves, respectively.

Subsequently, disturbance compensation can be done after the open-loop estimation is realized. The compensation simulation is carried out in two perpendicular radial degrees of freedom and axial degree of freedom, respectively. And the amplitude and frequency of disturbance forces change as before. As can be seen in Fig.8, disturbance rejection ability is enhanced when ESO is added into original PID feedback control.

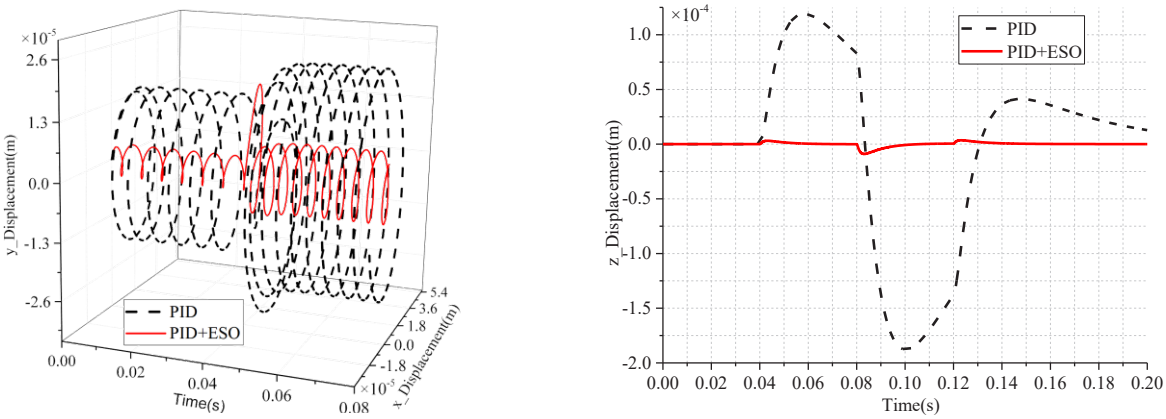

Fig.8 Simulation results of compensation performance in radial (left) and axial (right) degree of freedom. The displacement values with and without ESO are plotted with solid (red) and dashed (black) curves, respectively.

4.2 Characteristics of ESO

As mentioned before, with bandwidth concept introduced and some major parameters determined, the only unknown parameter of ESO is ω . Here the characteristics of ESO are elaborated through frequency response simulation.

In open-loop estimation condition, sinusoidal disturbances with different frequencies are exerted to AMB. Then the relationship between actual disturbance and estimated ones can be obtained in Fig.10 (left one). The unit of horizontal axis is converted to r/min, since disturbances are emulated as centrifugal forces from unbalance masses.

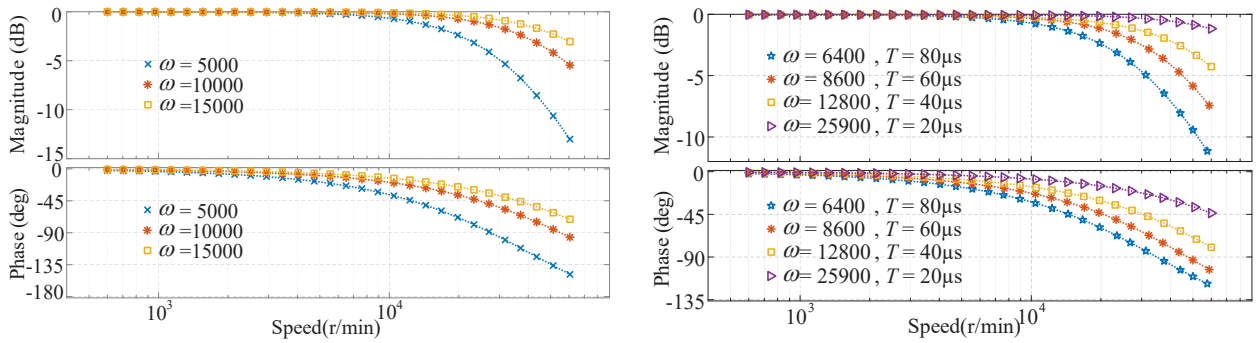

Fig.10 Open-loop frequency responses of ESO with different parameter values. The left figure shows the frequency responses of ESO with different values of ω , and the control period of ESO is T=30μs. The right figure shows the frequency responses with different values of ω and T, of which each ω is optimal for corresponding T.

As can be seen, with the frequency of disturbance increasing, the amplitude-frequency and phase-frequency curves both own a downward tendency, which means estimation errors will increase in aspects of amplitude and phase. Therefore, the compensation performance will be worse if the frequencies of disturbances are high enough. At the same time, we can conclude that, with larger values of ω , the estimation performance of ESO will be much better.

However, as is elaborated in Section 2, ω owns a stability margin related to control period T, and we can find that estimated value will be oscillated when ω is large enough in simulation. Therefore, the estimation accuracy of ESO is also effected by the control period. Different stability margins with different control periods are obtained in simulation as illustrated in Fig.11. It can be verified that with longer control period, the stability margin becomes smaller, which is in accordance with theoretical analysis in Section 2. Since the time delay of sampling and calculation is ignored in theoretical analysis, the numerical relationships between stability margin and control period are different in theoretical derivation and simulation. Nevertheless, the relationships are qualitatively coincident.

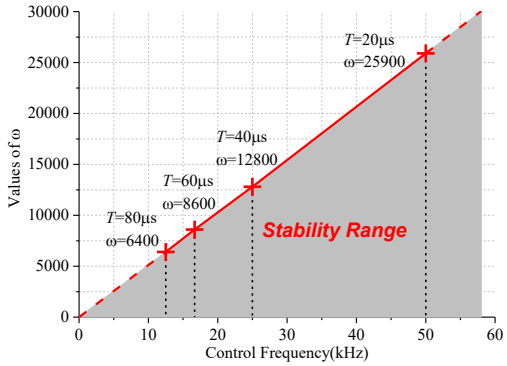

Fig.11 Stability margins with different control frequencies. Four different control periods are adopted (red crosses), and corresponding stability margins are fitted. The stability range can be derived which is displayed by shaded area.

Last but not least, if the value of ω is at its stability margin for each control period, different estimation performance can be obtained, which is illustrated in Fig.10 (right one). As is shown that, the larger value of ω with shorter control period, the better ESO estimates.

Above all, with shorter control period, the stability margin of ESO is larger; with larger value of ω , the estimated accuracy of ESO will be better.

5. Experiment verification

As described in Section 3, experiment verification was carried out on an AMB supporting centrifugal compressor. With PID feedback levitation control, the compressor worked well at 50,000r/min, and the input power of the motor was 9kW. Based on this, ESO is designed and realized in DSP. In order to protect the compressor from damaging, the rotor shaft is suspended in static state. And different disturbance currents are exerted in control windings to emulated as disturbance forces. Because of this, estimation accuracy verifications can be carried out on the platform.

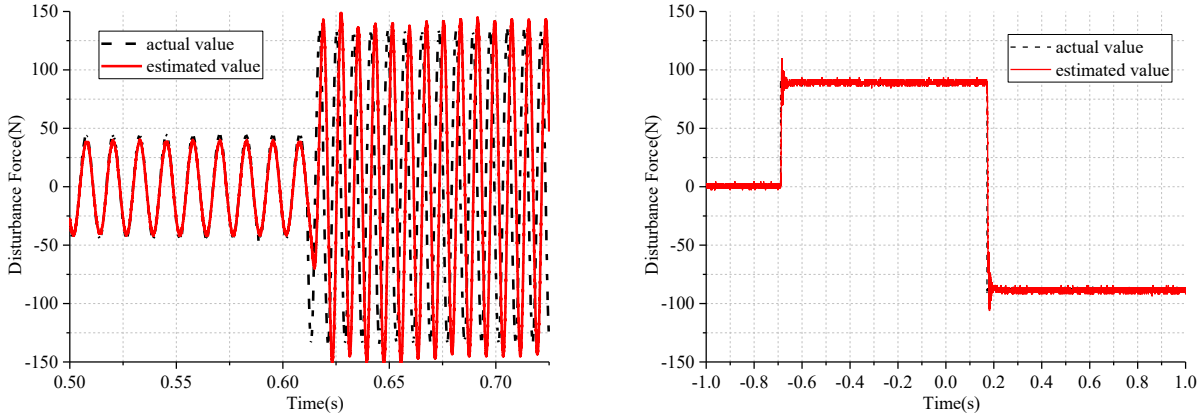

Fig.12 Experimental results of disturbance estimation in radial (left) and axial (right) degree of freedom. Actual and estimated values are plotted with the dashed (black) and solid (red) curves, respectively.

In radial degree of freedom, we exert sinusoidal disturbances like simulation. The frequency changes from 80 to 125Hz, and the amplitude of disturbance force from 48N to 130N. And step disturbances (±87.5N) are exerted in axial degree of freedom. The experiment results are shown in Fig.12.

Subsequently, disturbance compensation can be done after the open-loop estimation is realized. The compensation is carried out in a radial and the axial degree of freedom, respectively. And the disturbance forces are same as before. As can be seen in Fig.13, disturbance rejection ability is enhanced when ESO is added into original PID feedback control.

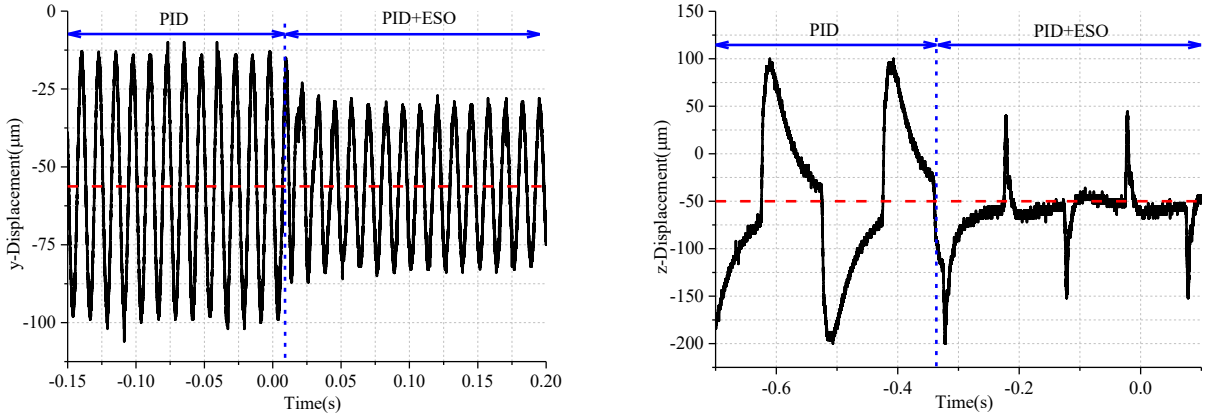

Fig.13 Experimental results of compensation performance in radial (left) and axial (right) degree of freedom. ESO is added into original PID controller at a time, which is labeled by short dash line (blue). Actual displacement fluctuations and ideal equilibrium positions are plotted with solid (black) and dash (red) curves, respectively.

Because of time constraints, we have not shorten control period in experiment, which is T=80μs. Therefore, the estimation accuracy and compensation performance are not ideal compared with simulation results (T=30μs).

6. Conclusions

This study investigated unbalance force observer and compensator for AMB supporting centrifugal compressors. It was aimed at disturbance rejection when suspended rotor shaft with abrupt load force changes or external disturbances forces. ESO was designed for AMB to realize disturbance estimation. Its parameter tuning method and characteristics were investigated through theoretical analysis and simulation. Finally, the estimation and compensation ability of ESO were validated on a suspended centrifugal compressor rig. It's worth mentioning that a method was adopted to verify estimation accuracy of ESO on a real platform.

We can conclude that, we could reduce calculation or improve sampling method to shorten control period, and the stability margin of ESO will be larger, which can improve the estimated accuracy and enhance the disturbance rejection ability of ESO.

References

Schweitzer, G., & Maslen, E. H. Magnetic bearings: theory, design, and application to rotating machinery (2009).

Han, J. From PID technique to active disturbances rejection control technique. Basic Automation (2002). (in Chinese)

Han, J. Auto-disturbances-rejection controller and its applications. Control & Decision (1998). (in Chinese)

Alexander, B. X. S., Rarick, R., & Dong, L. A novel application of an extended state observer for high performance control of NASA's HSS Flywheel and fault detection. American Control Conference (2008), pp.5216 - 5221.

Wang, X., & Ding, Q. Levitation decoupling control for permanent-magnet bearingless synchronous motors based on speed information observation. Control Theory & Applications, Vol. 28, No. 12 (2011), pp. 1803-1807. (in Chinese)

Wang, X., & He, P. Stability analysis and verification for bearingless magnetic levitation system with disturbance rejection. Control Theory & Applications, Vol. 29, No. 5 (2012), pp. 665-672. (in Chinese)

Zhou, Z., Qu, Y., & Yang, J. Levitation control of a planar magnetic bearing based on improved ADRC. Transactions of China Electrotechnical Society, Vol. 25, No. 6 (2010), pp. 31-38. (in Chinese)

Zhou, Z., Yang, J., Qu, Y., & Liu, D. Horizontal thrust control of magnetic suspension platform based on active disturbance rejection controller. Journal of Mechanical Engineering, Vol. 44, No. 9 (2008), pp. 193-199. (in Chinese)

Li, K., Deng, Z., Liu, C., & Hua, C. Design of disturbance rejection control system for 5-dof magnetic bearing. Journal of Aerospace Power, Vol. 30, No. 4 (2015a), pp. 1016-1024. (in Chinese)

Li, K., Deng, Z., Liu, C., & Zhou, J. Design of fuzzy controller with linear extended state observer for magnetic suspension bearings. IEEE International Conference on Electrical Machines and Systems. (2015b).

Gao, Z. Active disturbance rejection control: a paradigm shift in feedback control system design. American Control Conference (2006).